Liver $T_1\rho$ MRI measurement in healthy human subjects at 3 T: a preliminary study with a two-dimensional fast-field echo sequence

M DENG, MMed, F ZHAO, MMed, J YUAN, PhD, A T AHUJA, FRCR and Y-X J WANG, MMed, PhD

Department of Imaging and Interventional Radiology, Prince of Wales Hospital, The Chinese University of Hong Kong, Shatin, Hong Kong SAR, China

Objectives: The aim of this study was to explore the technical feasibility of $T_1\rho$ MRI for the liver, and to determine the normal range of liver $T_1\rho$ in healthy subjects at clinical 3 T.
Methods: There were 15 healthy volunteers. Three representative axial slices were selected to cut through the upper, middle and lower liver. A rotary echo spin-lock pulse was implemented in a two-dimensional fast-field echo sequence. Spin-lock frequency was 500 Hz, and the spin-lock times of 1, 10, 20, 30, 40 and 50 ms were used for $T_1\rho$ mapping. The images were acquired slice by slice during breath-holding. Regions of interest (ROIs; $n=5$) were manually placed on each slice of the liver parenchyma region, excluding artefacts and vessels. The mean value of these ROIs ($n=15$) was regarded as the liver $T_1\rho$ value for the subject. Six subjects were scanned once at fasting status; six subjects were scanned once 2 h post meal; three subjects were scanned twice at fasting status; and seven subjects were scanned twice 2 h post meal.
Results: When two readers measured the same 10 data sets, the interreader reproducibility (ICC: intraclass correlation coefficient) was 0.955. With the 10 subjects scanned twice, the ICC for scan–rescan reproducibility was 0.764. There was no significant difference for the liver $T_1\rho$ value at the fasting status (43.08 ± 1.41 ms) and post-meal status (42.97 ± 2.38 ms, $p=0.867$). Pooling together all the 32 scans in this study, the normal liver $T_1\rho$ value ranged from 38.6 to 48.3 ms (mean 43.0 ms, median 42.6 ms).
Conclusion: It is feasible to obtain consistent liver $T_1\rho$ measurement for human subjects at 3 T.

Received 31 May 2011
Revised 26 July 2011
Accepted 30 August 2011

DOI: 10.1259/bjr/98745548

© 2012 The British Institute of Radiology

Chronic liver disease is a major public health problem worldwide. Chronic liver disease and cirrhosis result in about 35 000 deaths each year in the USA. The trend is expected to increase owing to an aging population, the growing epidemic of obesity and non-alcoholic steatohepatitis, and the continued emergence of clinical manifestations among individuals with long-standing chronic hepatitis C infection [1, 2]. Liver fibrosis, a common feature of almost all causes of chronic liver disease, involves the accumulation of collagen, proteoglycans and other macromolecules within the extracellular matrix. The accumulation of proteins in the extracellular matrix promotes the formation of scars that bridge together adjacent portal triads and central veins. Ultimately, progressive hepatic fibrosis leads to cirrhosis, in which fibrous bands carve the liver parenchyma into nodules of regenerating hepatocytes, a characteristic feature of almost all end-stage liver disease [3]. Clinically, liver fibrosis usually has an insidious onset and progresses slowly over decades. Patients remain asymptomatic or have only mild, non-specific symptoms until the development of cirrhosis. Originally considered to be irreversible, hepatic fibrosis is now regarded as a dynamic process, with potential for regression [3]. Sustained virological response to treatment for chronic hepatitis B or chronic hepatitis C is associated with improvement in histological scores for fibrosis [4]. Even cirrhosis is reversible, as demonstrated by a recent study on patients with chronic biliary obstruction [5]. Promising new treatments for liver fibrosis are under investigation in clinical trials [6].

While the majority of complications from chronic liver disease result from progressive hepatic fibrosis, the available diagnostic tests used in clinical practice are not sensitive or specific enough to detect occult liver injury at early or intermediate stages [7, 8]. Liver biopsy is the standard of reference for diagnosis and staging of liver fibrosis. However, it is an invasive procedure, with possible side complications. It can lead to hospitalisation in 3% of cases, and has a fatality rate of 0.03% [9]. Histological assessment of fibrosis is also an inherently subjective process, and subject to sampling variability. A study that compared laparoscopic *vs* histological diagnosis of cirrhosis found that 32% of cases were underdiagnosed with histological examination of a single liver

Address correspondence to: Dr Yi-Xiang J Wang, Department of Imaging and Interventional Radiology, Prince of Wales Hospital, The Chinese University of Hong Kong, Shatin, NT, Hong Kong SAR, China. E-mail: yixiang_wang@cuhk.edu.hk
This study is supported by a direct grant for research from the Chinese University of Hong Kong (2041607), by Hong Kong ITF grant ITS/021/10 and partially by a grant from the Research Grants Council of the Hong Kong SAR (project no. SEG CUHK02).
M Deng and F Zhao contributed equally to this study.

biopsy specimen [10]. Also, a number of studies have demonstrated excessive histological sampling error (25–40%), resulting in poor reproducibility regardless of underlying liver disease origin [11]. In addition, interpretation variation by expert histopathologists may be as high as 20% [12]. These limitations make liver biopsy unsuitable for diagnosis and longitudinal monitoring in the general population. A reproducible and reliable non-invasive method is needed to evaluate disease progression in patients with chronic liver disease, to monitor treatment with conventional drugs and new drugs under development, and for epidemiological research. It has been noted that the absence of robust non-invasive markers is the most significant barrier to clinical trial development for novel pharmacological strategies to combat hepatic fibrosis [13].

With a biliary duct ligation-induced liver fibrosis rat model, we reported that $T_1\rho$ MRI is able to detect liver fibrosis, and the degree of fibrosis is correlated with the degree of elevation of the $T_1\rho$ measurements [14]. Additionally, our recent study demonstrated $T_1\rho$ MRI can be used to assess liver fibrosis induced with CCl4 intoxication of 1 ml kg^{-1} twice weekly. At week 2, week 4 and week 6, the rat liver $T_1\rho$ had a value increased over the baseline value by 12.0%, 16.5% and 23.0%, respectively. While at 4 weeks after the withdrawl of CCl4 insult, liver $T_1\rho$ decreased to close to the baseline value (only 2.3%, higher than the baseline value) [15]. These results suggest liver $T_1\rho$ quantification may play an important role for liver fibrosis early detection and grading. To translate liver $T_1\rho$ MRI to a clinically applicable imaging biomarker [16], this study was carried out with three aims: (1) to establish a clinical applicable method for liver $T_1\rho$ MRI measurement and assess its scan–rescan reproducibility, (2) to investigate whether liver $T_1\rho$ MRI value differs between the fasting status and post-meal status; and (3) to get the normal liver $T_1\rho$ MRI range in healthy subjects at 3 T.

Methods and materials

All volunteers were recruited from an advertisement in a university. The study was approved by the institutional ethics committee, with all subjects providing informed signed consent. All subjects were clinically healthy, with no liver disease history or alcoholism. After the MRI examination, the subjects were followed up by telephone for 3 months and confirmed they remained healthy. In total, 15 subjects took part in this study, comprising 8 males and 7 females, with a mean age of 28 years (range: 20–44 years). Subjects were asked to undergo MRI 2 h after their standard evening meal, and/or early in the morning before taking breakfast (fasting status), depending on their availability.

MRI data acquisition was performed on a 3 T clinical scanner (Achieva; Philips Healthcare, Best, Netherlands). An 8-channel cardiac coil was used as the signal receiver to cover the liver, and the built-in body coil was used as the signal transmitter. Subjects were examined supine. Anatomical imaging protocol was axial breath-hold T_2 weighted spectral adiabatic inversion recovery (SPAIR) sequence (repetition time, TR=1236 ms; echo time, TE=70 ms; 300×170 matrix; voxel size=1×1.4×7 mm; 20 slices; section thickness 7 mm; intersection gap 2 mm; number of signal averages, NSA=2). After inspection of the anatomical images revealed no imaging abnormalities, with scout scans in the coronal plane and sagittal plane, three representative axial slices were selected to cut through the upper, middle and lower liver for $T_1\rho$ imaging (Figure 1). Volume shimming was employed to minimise B0 inhomogeneities.

For $T_1\rho$ measurement, a rotary echo spin-lock pulse was implemented in a two-dimensional fast field echo (FFE) sequence [17]. Spin-lock frequency was set as 500 Hz and spin-lock times of 1, 10, 20, 30, 40 and 50 ms were used for $T_1\rho$ mapping. Segmented normal phase alternating FFE readout was used for acquisition. $T_1\rho$ weighted images were acquired during the transient status towards the steady state, but with $T_1\rho$ weighted magnetisation maintained [18]. A rotary echo spin-lock pulse was applied once for every segment length of 80 readouts. A delay time of 6000 ms was inserted after each segment acquisition to fully restore the equilibrium magnetisation prior to the next $T_1\rho$ preparation (Figure 2). TE and TR for FFE acquisition were 1.16 and 2.3 ms, respectively. The voxel size was 1.50×1.50×7.00 mm. The flip

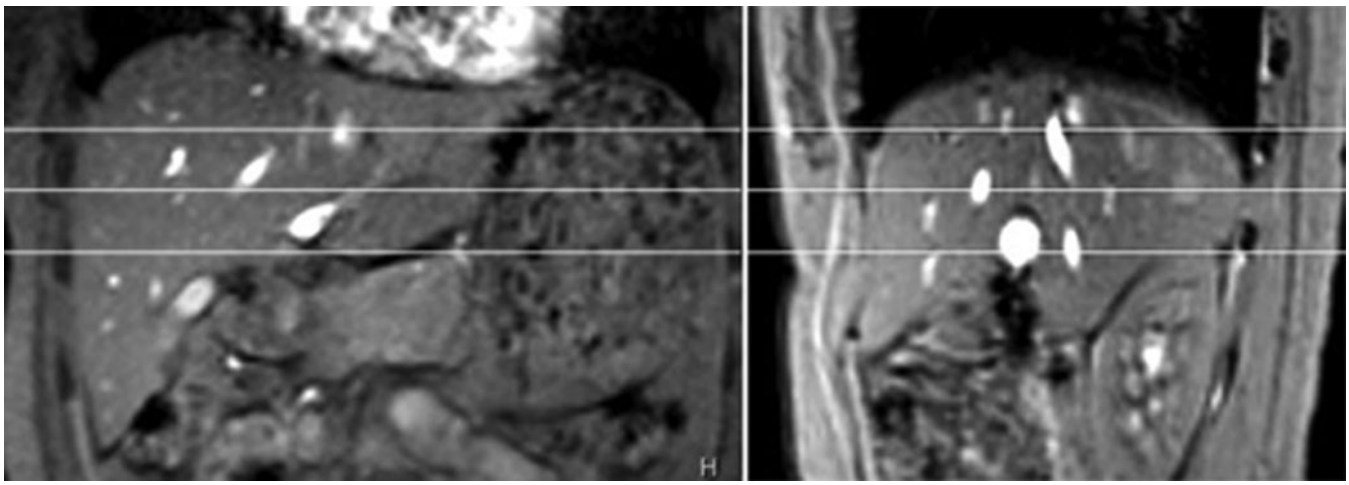

Figure 1. (a) Coronal and (b) sagittal scout images. Three axial slices are selected to cut through the upper, middle and lower liver.

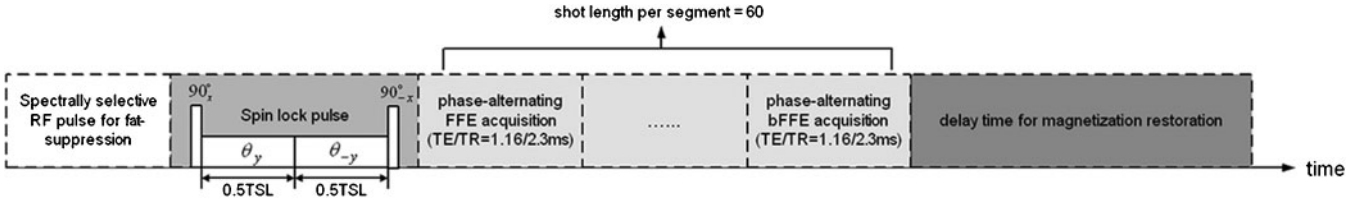

Figure 2. Diagram of the spin-lock fast field echo (FFE) imaging sequence for $T_1\rho$ image. TSL, time of spin-lock pulse.

angle was 40° and the NSA was 2. A sensitivity-encoding (SENSE) factor of 1.5 was applied for parallel imaging to reduce the phase-encoding steps, and hence the acquisition time. The whole body specific absorption rate (SAR) was $<0.4\,W\,kg^{-1}$ for this sequence as demonstrated on the scanner's console.

The images were acquired with a breath-hold technique. Volunteers were trained to breath-hold during shallow breathing, and maintain breath-holding at a similar breathing depth. At each slice level, $T_1\rho$ images of each spin-lock time were inspected immediately after acquisition, images with a breath-holding position shift were discarded and these images were reacquired. The scan time was 26 s per spin-lock time point (about 3 min for six spin-lock time points). The actual data acquisition time which needed breath-holding was 8 s per spin-lock time point. The scan time of conventional T_2 weighted image was 24 s. Including the time for rescanning, the whole examination lasted about 15 min.

$T_1\rho$ maps were computed on a pixel-by-pixel basis using a mono-exponential decay model with a home-made Matlab program (Mathworks, Natick, MA):

$$M(TSL) = M0 \times \exp(TSL/T_1\rho) \quad (1)$$

Where M0 and M(TSL) denote the equilibrium magnetisation and $T_1\rho$-prepared magnetisation with the spin-lock time of TSL, respectively.

This mono-exponential equation was linearised by logarithm and $T_1\rho$ maps were generated by fitting all pixel intensity data as a function of TSL using linear regression. $T_1\rho$ was calculated as –1/slope of the straight-line fit. Maps of coefficient of determination (R^2) were also generated for the evaluation of goodness of fit. Only $T_1\rho$ values for pixels associated with $R^2>0.80$ were included in the subsequent region of interest (ROI) placement and $T_1\rho$ analysis to eliminate the unreliable poorly fitted $T_1\rho$ values due to the blood vessel contamination with fresh blood inflow, as well as respiration-induced artefacts.

The data were analysed by two radiology trainees (DM, FZ) with more than 3 years of experience of reading abdominal MRIs. To quantify liver $T_1\rho$ value, five ROIs of approximately 100–200 mm^2 were manually placed on the liver parenchyma region of each slice's $T_1\rho$ maps with $R^2>0.80$, excluding observable artefacts and blood vessels (Figure 3), leading to a total of 15 ROIs from each liver examination. The mean value of these 15 ROIs was regarded as the liver $T_1\rho$ value for the subject. The first 10 data sets from post-meal status were used to assess interreader reproducibility. For this, the data were assessed by two readers independently. After the confirmation of satisfactory interreader reproducibility, the remaining data were measured by one trainee only (DM), and the results by this trainee were used for further analysis and processing.

Data are presented as mean ± standard deviation. Reproducibility was assessed using intraclass correlation coefficient (ICC) on absolute agreement. According to Fleiss [19], an ICC value of <0.4 represents poor agreement, a value >0.75 represents good agreement and a value between 0.4 and 0.75 represents fair to moderate agreement. Comparison of liver $T_1\rho$ value at fasting status and post-meal status was carried out with Mann–Whitney *U*-test. All statistical analyses were done using SPSS v. 14.0 (SPSS, Chicago, IL). A *p*-value <0.05 was considered statistically significant.

Results

In total 32 scans were performed. Six subjects were scanned once at fasting status; six subjects were scanned once 2 h post-meal; three subjects were scanned twice at fasting status; and seven subjects were scanned twice 2 h post-meal. Satisfactory liver $T_1\rho$ maps (Figure 4), as well as conventional T_2 weighted images, were obtained from all the scans. Using the threshold of $R^2=0.8$, around 10–20% of liver pixels (including pixels for blood vessels) were excluded (Figure 4). One subject had mild claustrophobia, but his images remained satisfactory. The liver $T_1\rho$ values of these 32 scans are listed in Table 1.

The ICC for interreader measurement reproducibility was 0.955, indicating good reproducibility between the two readers. 10 subjects were scanned twice (3 at fasting status and 7 post meal); the ICC for scan–rescan

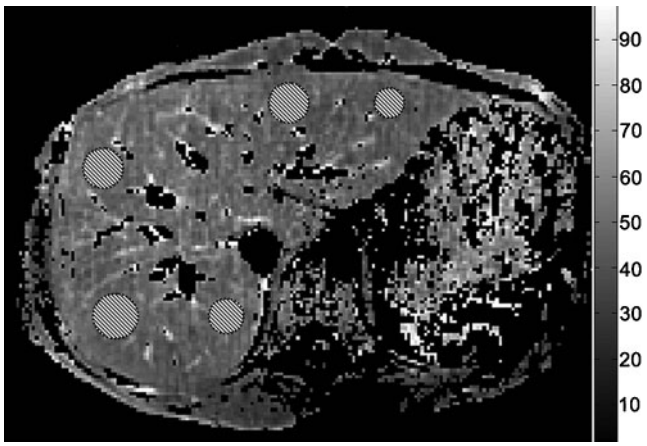

Figure 3. $T_1\rho$ map with coefficient of determination $R^2>0.8$ evaluation. Five regions of interest are placed on the liver parenchyma region, excluding observable artefacts and blood vessels.

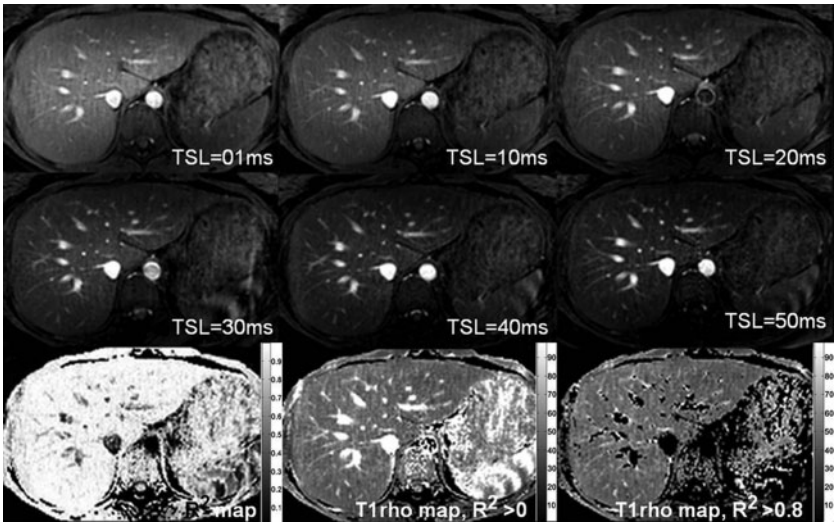

Figure 4. The upper and middle rows show liver $T_1\rho$ weighted images acquired with spin-lock times (TSL) ranging from 1 to 50 ms. Note vessels demonstrate high signal on $T_1\rho$ weighted images. The lower row shows the coefficient of determination (R^2) map (left), the $T_1\rho$ map without R^2 evaluation (middle) and the $T_1\rho$ map with $R^2>0.8$ evaluation (right).

reproducibility was 0.764, indicating good reproducibility (Table 1).

A comparison was made to see whether there was a difference in the liver $T_1\rho$ value at the fasting status and at post meal. For those scanned twice, only the data from the first scan were used, resulting in 9 values from fasting status and 13 values from post meal status. Liver $T_1\rho$ value was 43.1 ± 1.4 ms in the fast status and 43.0 ± 2.4 ms in the post meal status. There was no significant difference in their values ($p=0.867$).

Pooling all the 32 scans in this study, liver $T_1\rho$ values ranged from 38.6 to 48.3 ms. The mean value was 43.0 ± 2.2 ms and the median value was 42.6 ms.

Discussion

In patients with pre-cirrhotic stages of liver fibrosis, as well as patients with early cirrhosis, the liver parenchyma usually has a normal appearance, or may exhibit only subtle, non-specific heterogeneity on conventional MRI. Recently, a number of novel MRI techniques have been investigated to identify or grade liver cirrhosis. These include double contrast-enhanced MRI [20], MR elastography [8, 21] and diffusion-weighted imaging [8, 22]. These techniques' sensitivity for early liver fibrosis, reproducibility and intersite variability have not been well established [23]. Other imaging methods, including ultrasound and nuclear imaging techniques, have limited value in detecting early liver fibrosis.

Recently, a new mechanism for MR tissue contrast, $T_1\rho$, has been investigated in biomedical applications. $T_1\rho$ represents the spin lattice relaxation time constant in the rotating frame, which determines the decay of the transverse magnetisation in the presence of a ''spin-lock'' radiofrequency field. $T_1\rho$ is sensitive to both low-frequency motional processes and static processes, so can be used to investigate macromolecular composition and proton exchange within tissues [24]. $T_1\rho$ has been proposed to be sensitive to the macromolecular composition of tissues [25–30]. $T_1\rho$ relaxation occurs in the presence of a spin-lock pulse that minimises the effects of diffusion and susceptibility on the signal. $T_1\rho$ MRI is a truly non-invasive technique; it does not involve additional intravenous injection or external driver such as in the case of elastography, therefore it can potentially have

Table 1. Liver $T_1\rho$ values of healthy volunteers

	$T_1\rho$ value (m)			
Case number	Scan 1—fasting	Scan 2—fasting	Scan 1—post meal	Scan 2—post meal
1	45.2	47.3	44.9	43.4
2	41.8	41.0	39.3	38.6
3	44.8		42.3	
4			48.3	45.8
5	42.4		41.6	41.6
6	42.3		39.8	
7	43.7	43.2		
8			41.2	41.0
9			44.8	42.7
10	41.3			
11			43.2	
12	42.0		42.7	46.4
13			44	
14	44.2		44.3	
15			42.5	
Mean	43.1 ($n=9$)	43.8 ($n=3$)	43.0 ($n=13$)	42.8 ($n=7$)

good reproducibility and some intersite agreement. Liver fibrosis involves the accumulation of collagen, proteoglycans and other macromolecules. It is plausible that $T_1\rho$ MRI may be sensitive for evaluation of liver fibrosis.

The technical difficulties of $T_1\rho$ MRI include its relatively slow acquisition speed, sensitivity to B0 and B1 field inhomogeneities and high SAR. A rotary echo pulse was applied in this study to compensate the B1 inhomogeneities [17]. Volume shimming was also employed to minimise the B0 inhomogeneities. In all $T_1\rho$ scans in this study, SAR deposition was under the allowable Food and Drug Administration limits of $0.4\,W\,kg^{-1}$ averaged over the whole body [31]. Owing to respiratory motion, liver imaging represents a particular challenge for this technique. In our initial pilot studies, three-dimensional FFE sequence and respiratory gating was used to increase liver coverage; however, the upper and lower sections of the scan block tended to have poor image quality, probably due to B1 field inhomogeneity. Importantly, it was observed that even the use of respiratory gating might not completely eliminate the respiration-induced displacement of images acquired at each spin-lock time. Meanwhile, liver vessels displayed high signal intensities with the use of FFE sequence (Figure 4). Thus, even mild spatial misregistration due to respiratory motion could lead to an artificially high $T_1\rho$ value for liver parenchyma. As such, the criterion of $R^2>0.80$ was applied to eliminate the unreliable artificially high $T_1\rho$ values induced by the vessel contamination, as well as respiration-induced artefacts. Interestingly, the small sensor balloon placed on the abdominal skin surface for respiratory gating induced B0 field inhomogeneities and deteriorated image quality for the liver parenchyma region near the balloon. During pilot studies, we also hypothesised that coronal or sagittal image acquisition would be less affected by respiration as its movement is mostly in the cephalad–caudad direction. However, our results showed both coronal and sagittal imaging still suffered from respiratory motion, and also added cardiac motion artefact to coronal imaging. It is known that the liver would have a higher level of glycogen post meal than at fast status. Our current study suggests that this glycogen level fluctuation does not affect liver $T_1\rho$ level measurement.

The $T_1\rho$ imaging protocol may be further optimised in future studies. The scan time of $T_1\rho$ imaging was relatively long in the current study, and a good breath-hold is needed for a satisfactory result. Only three slices were acquired in this study for $T_1\rho$ imaging, though most chronic liver diseases would be diffusely distributed. The coverage of more slices has to be compromised with spatial resolution and signal-to-noise ratio within the acceptable scan time in practical clinical settings. One major factor that prolongs the $T_1\rho$ imaging time is the long delay time for equilibrium magnetisation restoration for any multishot segmented acquisition sequences. A relatively long delay time of 6000 ms was used in the current study to ensure the complete restoration of equilibrium magnetisation, as well as the lower SAR level. Longer shot length and fewer shot numbers might be beneficial for scan time reduction, whereas the SAR level would increase and the mono-exponential $T_1\rho$ weighting could be obscured with the approach to a steady state [32]. The mono-exponential model of $T_1\rho$ relaxation can be linearised by logarithm. In principle, only two spin-lock times are sufficient for linear fitting of $T_1\rho$ provided that the $T_1\rho$ weighted images acquired at these two spin-lock times have sufficiently high signal-to-noise ratios. Therefore, $T_1\rho$ imaging with fewer spin-lock time points is worth exploring in the future study. Additionally, three-dimensional data acquisition techniques with good respiration compensation are being pursued in our laboratory.

In conclusion, our study demonstrated it is feasible to obtain consistent liver $T_1\rho$ measurement for human subjects at 3 T. There was no difference in liver $T_1\rho$ values at fasting status and post-meal status. These preliminary results will be relevant for translating liver MRI $T_1\rho$ to a clinically applicable imaging biomarker for liver fibrosis.

References

1. Davis GL, Albright JE, Cook SF, Rosenberg DM. Projecting future complications of chronic hepatitis C in the United States. Liver Transpl 2003;9:331–8.
2. Charlton M. Nonalcoholic fatty liver disease: a review of current understanding and future impact. Clin Gastroenterol Hepatol 2004;2:1048–58.
3. Wallace K, Burt AD, Wright MC. Liver fibrosis. Biochem J 2008;411:1–18.
4. Leung NW, Lai CL, Chang TT, Guan R, Lee CM, Ng KY, et al. Extended lamivudine treatment in patients with chronic hepatitis B enhances hepatitis B e antigen seroconversion rates: results after 3 years of therapy. Hepatology 2001;33: 1527–32.
5. Hammel P, Couvelard A, O'Toole D, Ratouis A, Sauvanet A, Flejou JF, et al. Regression of liver fibrosis after biliary drainage in patients with chronic pancreatitis and stenosis of the common bile duct. N Engl J Med 2001;344:418–23.
6. Oh MK, Winn J, Poordad F. Review article: diagnosis and treatment of non-alcoholic fatty liver disease. Aliment Pharmacol Ther 2008;28:503–22.
7. Afdhal NH, Nunes D. Evaluation of liver fibrosis: a concise review. Am J Gastroenterol 2004;99:1160–74.
8. Talwalkar JA, Yin M, Fidler JL, Sanderson SO, Kamath PS, Ehman RL. Magnetic resonance imaging of hepatic fibrosis: emerging clinical applications. Hepatology 2008;47: 332–42.
9. Janes CH, Lindor KD. Outcome of patients hospitalized for complications after outpatient liver biopsy. Ann Intern Med 1993;118:96–8.
10. Poniachik J, Bernstein DE, Reddy KR, Jeffers LJ, Coelho-Little ME, Civantos F, et al. The role of laparoscopy in the diagnosis of cirrhosis. Gastrointest Endosc 1996;43: 568–71.
11. Ratziu V, Charlotte F, Heurtier A, Gombert S, Giral P, Bruckert E, et al. Sampling variability of liver biopsy in nonalcoholic fatty liver disease. Gastroenterology 2005;128: 1898–906.
12. Bravo AA, Sheth SG, Chopra S. Liver biopsy. N Engl J Med 2001;344:495–500.
13. Friedman SL, Bansal MB. Reversal of hepatic fibrosis: fact or fantasy? Hepatology 2006;43(2 Suppl 1):S82–8.
14. Wang YX, Yuan J, Chu ES, Go MY, Huang H, Ahuja AT, et al. $T_1\rho$ MR imaging is sensitive to evaluate liver fibrosis: an experimental study in a rat biliary duct ligation model. Radiology 2011;259:712–9.
15. Wang YX, Zhao F, Deng M, Yuan J, Yu J. MRI T1ρ as an imaging biomarker for monitoring liver injury progression and regression: an experimental study in rats with carbon

tetrachloride intoxication. Proceedings of Korean Congress of Radiology annual meeting 2011 Seoul SS 30 AB-09.
16. Wang YX. Medical imaging in pharmaceutical clinical trials: what radiologists should know. Clin Radiol 2005;60:1051–7.
17. Charagundla SR, Borthakur A, Leigh JS, Reddy R. Artifacts in T(1rho)-weighted imaging: correction with a self-compensating spin-locking pulse. J Magn Reson 2003;162:113–21.
18. Li X, Han ET, Busse RF, Majumdar S. In vivo T(1rho) mapping in cartilage using 3D magnetization-prepared angle-modulated partitioned k-space spoiled gradient echo snapshots (3D MAPSS). Magn Reson Med 2008;59:298–307.
19. Fleiss JL. Reliability of measurement: the design and analysis of clinical experiments. New York, NY: John Wiley & Sons; 1986.
20. Aguirre DA, Behling CA, Alpert E, Hassanein TI, Sirlin CB. Liver fibrosis: noninvasive diagnosis with double contrast material-enhanced MR imaging. Radiology 2006;239: 425–37.
21. Salameh N, Larrat B, Abarca-Quinones J, Pallu S, Dorvillius M, Leclercq I, et al. Early detection of steatohepatitis in fatty rat liver by using MR elastography. Radiology 2009;253:90–7.
22. Bonekamp S, Kamel I, Solga S, Clark J. Can imaging modalities diagnose and stage hepatic fibrosis and cirrhosis accurately? J Hepatol 2009;50:17–35.
23. Sirlin CB. Science to practice: can T_1 ρ imaging be used to diagnose and assess the severity of hepatic fibrosis? Radiology 2011;259:619–20.
24. Akella SV, Regatte RR, Gougoutas AJ, Borthakur A, Shapiro EM, Kneeland JB, et al. Proteoglycan induced changes in T_1 ρ—relaxation of articular cartilage at 4T. Magn Reson Med 2001;46:419–23.
25. Szyperski T, Luginbühl P, Otting G, Güntert P, Wüthrich K. Protein dynamics studied by rotating frame 15N spin relaxation times. J Biomol NMR 1993;3:151–64.
26. Knispel RR, Thompson RT, Pintar MM. Dispersion of proton spin-lattice relaxation in tissues. J Magn Reson 1974;14:44–51.
27. Duvvuri U, Goldberg AD, Kranz JK, Hoang L, Reddy R, Wehrli FW, et al. Water magnetic relaxation dispersion in biological systems: the contribution of proton exchange and implications for the noninvasive detection of cartilage degradation. Proc Natl Acad Sci USA 2001;98:12 479–84.
28. Nguyen AM, Johannessen W, Yoder JH, Wheaton AJ, Vresilovic EJ, Borthakur A, et al. Noninvasive quantification of human nucleus pulposus pressure with use of T_1rho-weighted magnetic resonance imaging. J Bone Joint Surg Am 2008;90:796–802.
29. Haris M, McArdle E, Fenty M, Singh A, Davatzikos C, Trojanowski JQ, et al. Early marker for Alzheimer's disease: hippocampus T_1rho estimation. J Magn Reson Imaging 2009;29:1008–12.
30. Nestrasil I, Michaeli S, Liimatainen T, Rydeen CE, Kotz CM, Nixon JP, et al. T_1rho and T_2rho MRI in the evaluation of Parkinson's disease. J Neurol 2010;257:964–8.
31. Collins CM, Li S, Smith MB. SAR and B1 field distributions in a heterogeneous human head model within a birdcage coil. Specific energy absorption rate. Magn Reson Med 1998;40:847–56.
32. Witschey WR, Borthakur A, Elliott MA, Fenty M, Sochor MA, Wang C, et al. T_1rho-prepared balanced gradient echo for rapid 3D T_1rho MRI. J Magn Reson Imaging 2008;28: 744–54.